Published in final edited form as:
J Cogn Neurosci. 2009 July ; 21(7): 1447–1460. doi:10.1162/jocn.2009.21005.

The Topography of Visuospatial Attention as Revealed by a Novel Visual Field Mapping Technique

Julie A. Brefczynski-Lewis, **Ritobrato Datta**, **James W. Lewis**, and **Edgar A. DeYoe**
Medical College of Wisconsin

Abstract

Previously, we and others have shown that attention can enhance visual processing in a spatially specific manner that is retinotopically mapped in the occipital cortex. However, it is difficult to appreciate the functional significance of the spatial pattern of cortical activation just by examining the brain maps. In this study, we visualize the neural representation of the "spotlight" of attention using a back-projection of attention-related brain activation onto a diagram of the visual field. In the two main experiments, we examine the topography of attentional activation in the occipital and parietal cortices. In retinotopic areas, attentional enhancement is strongest at the locations of the attended target, but also spreads to nearby locations and even weakly to restricted locations in the opposite visual field. The dispersion of attentional effects around an attended site increases with the eccentricity of the target in a manner that roughly corresponds to a constant area of spread within the cortex. When averaged across multiple observers, these patterns appear consistent with a gradient model of spatial attention. However, individual observers exhibit complex variations that are unique but reproducible. Overall, these results suggest that the topography of visual attention for each individual is composed of a common theme plus a personal variation that may reflect their own unique "attentional style."

INTRODUCTION

A simple and common way to think about visual attention is to envision it as a "spotlight" of enhanced neural activation within those regions of the brain that are particularly necessary to the performance of a task (Posner, Snyder, & Davidson, 1980). However, other studies suggest that allocation of attention may be more versatile than a simple spotlight. Intuitively, the spatial distribution of attention is different when one is reading text compared with monitoring airplanes in an air traffic control tower. Some attentional models have given the spotlight the ability to alter its range, expanding and contracting to meet the needs of a given task (Eriksen & Yeh, 1985; LaBerge, 1983). Others have noted that attention seems to spread beyond its intended target, sometimes falling off as a gradient or spreading to other locations within a quadrant, hemifield, gradient stripe, or to the boundaries of an object (Gobell, Tseng, & Sperling, 2004; Downing & Pinker, 1985; Hughes & Zimba, 1985; Duncan, 1984; Treisman, 1982).

Functional neuroimaging data from several laboratories, including our own, have demonstrated that cortical attentional enhancement can be spatially specific (McMains & Somers, 2005; Brefczynski & DeYoe, 1999a; Gandhi, Heeger, & Boynton, 1999; Tootell et al., 1998) or feature specific to regions of space with the feature of interest (Saenz, Buracas, & Boynton,

Reprint requests should be sent to Edgar A. DeYoe, Medical College of Wisconsin, MEB—Neurolab, 8701 Watertown Plank Rd., Milwaukee, WI 53226, or via, deyoe@mcw.edu.

2003). That is, attention enhances blood oxygenation level-dependent (BOLD) signals in areas of the visual cortex that correspond to the retinotopic location of an attended stimulus. Results from electrophysiological studies also suggest some level of spatial specificity, at least for the left and right hemifield (Heinze et al., 1994), but only at eccentricities under 10° (Seiple, Clemens, Greenstein, Holopigian, & Zhang, 2002). Regardless of the techniques used, it has been difficult to obtain a detailed appreciation of the topography of visuospatial attention, especially as it relates to the observer's view of the world. Thus, the details of the shape and size of the "spotlight" cannot be determined easily by examination of brain activation alone or by psychophysically probing a relatively small number of locations. Consequently, we developed a technique for visualizing the distribution of attention-related brain activation, as it would appear within the observer's field of view, and used this technique to examine the distribution of attention during different attention-demanding tasks. The resulting attentional field maps (AFMaps) provide a detailed picture of the attentional topography, its relationship to task-relevant factors, and its variation from individual to individual.

The following account of our findings is organized as two distinct experiments. The first experiment was designed to examine the attentional topography when subjects were cued to covertly attend to a single eccentric target within a dartboard-like array of distracter segments. This condition was alternated with passive fixation of a central marker. Based on our previous work, we predicted that attention directed to the target would enhance the appropriate retinotopic locations in the occipital cortex. More specifically, we predicted that the attentional effects would appear as a gradient in which the greatest level of enhancement would correspond to the cued location, gradually decreasing with distance (Downing & Pinker, 1985). In the second experiment, we examined the topography of attention as a function of the eccentricity of the attended target. Our hypothesis was that attentional enhancement would be highest at the attended target location as before, but that the spread of attentional enhancement would increase with eccentricity. Preliminary reports of this work have been presented previously (DeYoe, Brefczynski-Lewis, Datta, & Huddleston, 2004; Brefczynski & DeYoe, 1999a, 1999b; Brefczynski, Lewis, & DeYoe, 1999; DeYoe & Brefczynski, 1999).

METHODS

Methods and procedures common to all experiments are described below. Methods that were specific to each of the two main experiments are described separately in relevant sections.

Human Subjects

Volunteers with normal or corrected-to-normal vision (4 women and 10 men, all right-hand dominant) were recruited from the Medical College of Wisconsin faculty and student pool. Informed consent was obtained from all participants prior to scanning, in accordance with procedures and protocols approved by the Medical College of Wisconsin internal review board.

Stimulus

Visual stimuli were generated with a Cambridge Instruments VSG2/3 graphics board (Cambridge Research Systems, Kent, England). Participants viewed the computer graphics stimuli while in the magnetic resonance imaging (MRI) scanner via a custom-designed optical system (DeYoe et al., 1996), which allowed for a large field of view extending to 28° of eccentricity. The visual stimulus consisted of a dartboard-like array of counterphase flickering (8 Hz), striped (horizontal or vertical) and colored (orange or blue) segments whose outer boundary extended to 28° eccentricity (see Figure 1C). The colored stripes were roughly matched for luminance. The space average luminance of the stripe pattern (light and dark stripes) was roughly equivalent to the luminance of the gray background. In Experiment 1, there were six wedges and three rings (subtending eccentricity ranges of 1.0°–5.0°, 5.1°–12.7°,

12.8°–27.0°), totaling 18 segments. In Experiment 2, there were four rings (subtending eccentricity ranges of 0.4°–3.5°, 3.5°–7.0°, 7.1°–14.0°, 14.1°–27.0°), totaling 24 segments. The spatial frequency of the stripe patterns was scaled with the mean eccentricity of the segments. The color and orientation of each segment changed randomly every 2 sec, but ensuring that the number of occurrences of each of the four possible color/orientation combinations was matched for each scan run. A completely new randomization sequence was selected for each scan run to ensure that particular temporal sequences of stimuli would not be repeated across runs. (The software random number selection algorithm was "seeded" with random numbers derived from the system clock at the beginning of each scan run. Several hundred random numbers were initially "drawn" from the random number generator before using the numbers to generate stimuli in order to avoid potentially nonrandom sequences that can be obtained during the first few "draws" with some random number generators.)

Task

Participants were asked to continually fixate a small cross at the center of the stimulus array. They were cued to covertly attend to a particular target segment via pre-recorded auditory cues (spoken numbers) presented with custom electrostatic headphones (Koss, Milwaukee, WI). The visual task was to identify specific conjunctions of color and orientation at the attended target segment. Subjects were required to press one of two buttons if the conjunction was either blue/horizontal or orange/vertical. The other button was pressed for the other feature combinations (blue/vertical or orange/horizontal), each occurring 50% of the time. Cued attention trials were alternated with passive viewing trials for which sham button presses were made every 2 sec to match response-related activation of the motor cortex. Task timing information is illustrated schematically for the experiments in Figure 2 and is described in further detail in relevant sections below. Participants were trained for at least three runs on these tasks before functional magnetic resonance imaging (fMRI) data collection.

Eye Movements

An eye-position tracker (EyeLink II, SR research, LTD) was used to monitor eye fixation position while subjects performed the same attention task outside the scanner. Results are illustrated in Supplemental Figure 1, which shows that fixation was consistent and accurate when the subjects covertly attended to eccentric targets located to the left or right of fixation (Supplemental Figure 1A, left; Supplemental Figure 1B, small gray dots). For comparison, we recorded eye positions when subjects were asked to look directly at target segments to the left and right of center (Supplemental Figure 1A, right; Supplemental Figure 1B, black squares). Lateral eye movements during covert attention shifts were not significantly different when attending to left versus right targets, although there were slightly smaller deviations of eye position during passive fixation (0.4° average). This small difference did not account for our results, as subjects did not shift eye position to favor the attended target (Supplemental Figure 1B, gray dots).

Imaging Methods

Imaging techniques were similar to those described previously (Brefczynski & DeYoe, 1999a). Gradient-recalled, echo-planar fMRI was performed with a General Electric (Milwaukee, WI) Signa 1.5-Tesla MRI scanner equipped with a custom RF/gradient head coil (Medical Advances). Depending on the task, 14 to 17 axial slices were collected, each with 102 to 128 gradient-recalled echo-planar images (TE = 40 msec, TR = 2 sec, FA = 90°) with 3.75 × 3.75 × 6.0 mm resolution. At least two TR periods at the beginning of each scan were discarded to eliminate initial transients. Two additional TR periods at the end of each scan were often used to obtain an estimate of field homogeneity that was used in postprocessing to "unwarp" the fMRI images (Jesmanowicz, Wong, DeYoe, & Hyde, 1992). Anatomical images

were obtained using a T1-weighted spoiled gradient recalled at a steady state (GRASS) pulse sequence with a resolution of 256 × 192 and a slice thickness of 1.1 or 1.0 mm.

Retinotopic Mapping

Techniques for retinotopic mapping using temporal phase mapped, checkered annuli, and wedges (Figure 1A and B) have been described previously (DeYoe et al., 1996). Briefly, the mapping of visual field eccentricity was accomplished using a counterphase flickering (8 Hz), checkered annulus that slowly expanded from the center of gaze to 28° over a period of 40 sec. The expansion steps, inner and outer diameters, and check size were all scaled in proportion to the mean eccentricity of the annulus. To map visual field polar angle, a checkered hemifield (wedge) slowly rotated about the center of gaze. Both the annulus expansion and the hemifield rotation sequences were typically repeated five times in succession during an fMRI scan. Each stimulus evoked "waves" of activation that moved through the retinotopic visual cortex, activating successive retinotopic positions at different times (temporal phases) relative to the beginning of the stimulus cycle. In this manner, the retinal position of the stimulus that optimally activated a particular cortical locus could be determined from the time delay of its fMRI response. Valid responses were identified using a modification of a standard temporal cross-correlation method (Saad, 2000; Bandettini, Jesmanowicz, Wong, & Hyde, 1993). The modified algorithm efficiently identified the optimum temporal phase, the cross-correlation coefficient, and the magnitude of the response. The algorithm is available as the Hilbert Delay "plug-in" function in the analysis of functional neuroimages (AFNI) package (Cox, 1996).

Postprocessing

Most image postprocessing was performed with the AFNI analysis suite (Cox, 1996) and custom Unix scripts. Key postprocessing steps are outlined in more detail in the following sections.

Identifying Active Voxels—Raw fMRI *k*-space data were converted to images using a custom reconstruction technique (Jesmanowicz, Bandettini, & Hyde, 1998). The resulting images were assembled into volumetric datasets and then further processed using the AFNI analysis package. Individual images within the volumetric dataset were coregistered to reduce motion artifacts, and then further analyzed using several different methods depending on the task and stimulus presentation. For block design data, active voxels were detected using a modified correlation analysis (Bandettini et al., 1993) computed with the AFNI "FIM" function using a gamma model of the hemodynamic response function convolved with the timing of the attention condition blocks (cf. AFNI "waver" program; Figure 2A and B). The statistical significance of individual voxel responses at a given threshold for the correlation coefficient was computed as described in Cox, Jesmanowicz, & Hyde, 1995 and was read directly from the AFNI user interface.

Flatmap Construction—Data were projected onto flattened occipital–parietal lobes for five subjects of Experiment 1, using the public-domain software packages SureFit and Caret (http://brainmap.wustl.edu) (Van Essen et al., 2001). For flattening, a lateral cut was created roughly along the lateral occipital sulcus, such that the visual area boundaries run approximately perpendicular to the cut (black dotted and solid lines in Figure 3).

AFMap and ROImap Construction—To examine the detailed topography of attention, we displayed the attention-related brain activity as a back-projection onto the observer's visual field. Construction of such an attentional field map (AFMap) was performed via several stages as outlined in Figure 1. The retinotopic mapping data were used to determine the eccentricity and polar angle of the stimulus that maximally excited each visually responsive voxel (Figure 1A and B). For each responsive voxel, a circle symbol was placed at the corresponding

retinotopic location on a schematic diagram of the visual field (Figure 1D). The color of the symbol was then selected from a scale representing the amplitude of attention-related activation obtained for that voxel during the attention task (Figure 1C). The diameter of each circle was scaled to a 70% confidence interval for the true location based on a previous study by Saad (1996), in which the temporal variability of fMRI responses to comparable visual stimulation was characterized. In that study, the standard deviation in temporal phase delay across all responsive voxels in a sample from seven subjects was found to be 2.1 sec. For a temporal phase mapping paradigm with a 40-sec cycle period as used here, the 70% confidence interval for the estimated phase delay is thus 2.16 sec. The diameter of the circle symbol was then adjusted accordingly to reflect the corresponding range in mean eccentricity of the annulus mapping sequence. (Note that the range scales with eccentricity so that the symbols are smaller near the center of gaze. Accuracy in the polar angle dimension also scales with eccentricity, so for simplicity the symbols have been plotted as circles. We also assume that the temporal accuracy of fMRI phase measurements are uniform throughout the visually responsive cortex.) An accurately scaled outline of the stimulus array was superimposed on the AFMap to show the boundaries of the target and distracter segments.

To permit statistical analysis of differences in the topography of the AFMaps, we identified sets of voxels that retinotopically represented each stimulus segment and defined them as separate regions of interest (ROIs) within the visual field (as distinct from anatomically defined ROIs for different cortical areas). Each visual field ROI included all the circles whose centers fell within a given segment on the AFMap. We then averaged the responses of the voxels within each set. Next, we displayed the resulting averaged data in a format that was comparable to the AFMap by plotting the normalized mean intensity for each segment at its corresponding center location on a new visual field diagram, and then fit the data points with a smooth, continuous, pseudocolored surface. This surface was then viewed as a contour plot using the same color scale as for the AFMaps (Figure 1E). (We feel that a smoothed surface provides a more physiologically plausible view of the underlying physiology, so we prefer this format to a more discontinuous type of display in which each segment is displayed as a single uniform color with sharp borders. However, subsequent statistical analyses were based solely on the actual data values for each segment, not on the interpolated values used for display.)

Visual Area ROIs for AFMaps—For this study, only data from voxels with statistically significant activation ($p < .05$) for *both* polar angle and eccentricity mapping within the retinotopic occipital cortex were used to construct AFMaps and ROImaps. Except where indicated otherwise below, this typically encompassed medial, dorsal, and ventral occipital visual areas, including major portions of V1, V2, V3/VP, V4, and possibly other visual areas as defined in DeYoe et al. (1996). For five subjects, the retinotopic boundaries of several of these areas were verified on flat maps of the occipital cortex, but a detailed identification of all areas in all subjects was not performed. In this respect, it is important to note that it was generally not possible to construct AFMaps from individual visual areas beyond V1/V2 because they typically are not large enough to contain a sufficient number of voxels to create a good quality, well-populated AFMap.

Statistically Calibrated Color Scales—To identify statistically reliable attention-related activity in the AFMaps and ROImaps, we used a color scale that distinguished between attentional modulation values that were statistically different from zero and those that were nonsignificant.

For AFMaps, the statistical significance of individual voxel responses (each circle symbol) was based on the sampling distribution of the partial correlation coefficient computed using the AFNI “FIM” function. If the voxel’s response was significant, then its symbol color was scaled according to the FIM amplitude measure, “alpha,” which reflects the multiplicative

scaling factor needed to achieve a least squares best fit of the reference waveform to the actual fMRI time course (Cox, 2005). Statistically significant amplitude values were displayed in shades of red/yellow (positive: response greater than baseline) or blue (negative: response below baseline or anticorrelated with the reference waveform). Amplitude values were normalized to the mean of the top 5% of values. Amplitude values that were nonsignificant were colored one of four shades of gray/black to try to preserve some of the low-level spatial topography even though it was not statistically different from zero.

For ROImaps, we calculated the mean FIM amplitudes for all groups of voxels representing each segment in the stimulus array. *t* statistics were then computed for these individual pools of voxels representing each segment. Segments having a *t* value that differed significantly from zero ($p < .05$) were assigned a color on the basis of the mean normalized amplitude value. Segments with nonsignificant *t* values were colored in shades of gray/black as described above for the AFMaps. Data were normalized to the segment with the highest mean amplitude.

Stimulus and Task for Experiment 1

Each of five subjects fixated the center of the dartboard-like stimulus array (Figure 1C) while attending to an eccentric target segment located 10.5° to the right or left of fixation (middle segment on the left or right), as cued by an auditory signal. Cues were presented in blocks of eight trials (2 sec/trial) alternating with blocks of rest trials in which subjects passively fixated a central marker (sequence depicted schematically in Figure 2A). Four complete cycles of the block design were obtained during each of four to eight fMRI scans. The first and last cycles were removed to avoid artifacts at the beginning and end of each scan run. Six to eight retinotopy scans (half eccentricity, half polar angle mapping) were also obtained during the same scan session in order to construct AFMaps and ROImaps. During the “attend” conditions, subjects performed a feature conjunction task at the attended target as described above under Methods. Average accuracy of task performance was 80.7% correct and did not significantly differ for the attend-right and attend-left conditions.

Valid behavioral data for only four subjects were collected during the actual fMRI scan sessions (Subjects 1, 5, 6, and 7) due to an undetected software/hardware error (also present in Experiment 2). However, comparable behavioral data were obtained from all subjects performing the identical task outside the scanner.

Stimulus and Task for Experiment 2

In the second experiment, the stimulus, scanning parameters, and task were the same as described for Experiment 1, except for the following differences: The stimulus consisted of four rings of segments as described earlier. Five subjects performed the attention task which consisted of attending to a cued sequence of four target locations extending from most foveal to most peripheral along the right horizontal meridian (Figure 2B). Each target location in the sequence was cued for a block of five trials (2 sec/trial) and the whole sequence was repeated five times within each fMRI scan. The scan was itself repeated five times. Six to eight retinotopy scans were also obtained during the same scan session in order to construct AFMaps and ROImaps. Average accuracy of task performance was 84.3% and did not significantly differ for the four eccentric target locations.

RESULTS

Experiment 1: Attentional Distribution for Single Right or Left Targets

Figure 3 shows the pattern of attention-related brain activation for a single subject displayed on cortical flatmaps of the left and right occipital–parietal cortex. Attend-left (A) and attend-right (B) conditions resulted in attention-related modulation that was highest in retinotopic

visual areas of the contralateral hemisphere, as predicted. For example, in the right hemisphere of Figure 3A, attention directed to a target on the left produced a swath of activated foci (yellows and reds) extending through most occipital retinotopic areas (black lines in Figure 3 mark boundaries of visual areas that could be determined via standard retinotopic mapping techniques; DeYoe et al., 1996). Attentional activation is also shown extending into the temporal and parietal lobes. Similar effects were seen in the left hemisphere when attending to the right target (Figure 3B). In addition to the predicted enhancements in the visual cortex contralateral to the cued targets, some weak foci of enhancement were also seen in the hemisphere ipsilateral to the cued target, apparent in Figure 3 as darker red areas. Suppressive effects of attention (Figure 3, blue) were also observed in both hemispheres but particularly in more foveal regions of the contralateral hemisphere. All subjects showed similar overall patterns, including spatial specificity in the parietal cortex (data not shown).

Attentional Field Maps—Figure 4 illustrates the topography of the attentional activation from the retinotopically organized occipital cortex displayed as AFMaps and corresponding ROImaps computed as a group average (left) and as individual maps for each of five subjects. For all maps, yellow indicates strongest enhancement, light blue indicates strongest suppression, and signals not significantly different from zero are indicated in shades of gray/black. Circle symbols in the AFMaps were plotted in semi-sequential order, from nonsignificant values (grays) to negative values in order of magnitude, followed by positive values in the order of magnitude, such that the most intense positive voxels would be displayed on top. This has the effect of sometimes making it difficult to appreciate the mix of positive and negative effects at a given location, such that a few positive voxels plotted at the surface could result in the appearance of enhancement in an otherwise low or nonsignificant region. (We tried other plotting strategies but this approach produced AFMaps which intuitively appear to correlate best with the patterns observed in the averaged ROImaps.) Also note that the size of each circle symbol in the AFMaps provides an estimate of the potential measurement error in assigning a voxel to a given location in the field of view. Consequently, some voxels whose true retinotopic representation corresponds to a given target segment may have a symbol that extends partially outside the confines of the segment in the AFMap.

The group-average maps for the attend-right (Figure 4A) and attend-left (Figure 4B) conditions reveal the expected retinotopic specificity for target location, in that the strongest attentional enhancement was associated with the cued location (outlined in green in Figure 4). Comparing the individual AFMaps and ROImaps with the grand-average maps showed that the spread of enhancement to segments surrounding the cued target varied significantly across subjects and that attentional effects could sometimes be observed even in distant segments in the opposite visual field, consistent with the activation patterns observed in the cortex (Figure 3). However, the averaged ROImaps show that the strongest focus was virtually always at the attended target, although for some subjects equally strong activation could also appear at a nearby target (e.g., Subjects 4 and 5, attend-left condition). Other characteristics of the activation patterns in the visual field opposite the attended target varied across subjects and ranged from suppression (blue) to moderate activation (orange), with weak activation (red) often appearing spread across multiple locations (e.g., Subject 2). Overall, subjects appeared to vary in the “tightness” of attentional focus (Subjects 2 vs. 3) and in the complexity of low-level effects (Subjects 3 vs. 5).

The observed individual variation in attentional topography raised the possibility that the attentional topography of each observer reflects unique but consistent variations on a common average pattern. To explore this possibility further, we examined the consistency of the attentional patterns for two subjects in three separate scan sessions obtained months apart (Figure 5A). Note that the attentional topography tends to look more similar (although not identical) within subject than between subjects. For example, Subject 5 had a relatively diffuse

attentional topography and more enhancement in the ipsilateral visual field compared with the relatively tighter focus of Subject 2, even over a 12-month period. Also note the remarkable consistency in the distribution of strong attentional effects (yellow circles) in the AFMaps for Subject 5 over this 1-year period.

Consistency within an individual is further documented in Figure 5B (top row), which shows five datasets obtained from a single subject in one day. There is a consistent tendency for strong attentional activation to spread into the segment directly above the attended target (left center segment). However, there also appear to be important run-to-run differences in the overall spread of effects. Close examination reveals that these differences mainly reflect minor variations in nontarget segments from scan to scan, perhaps reflecting variations in overall sensitivity to attentional effects. Accordingly, we tried adjusting the color scale maximum and minimum to see if the apparent differences in topography might reflect a simple level and/or "gain" effect. Indeed, as shown in Figure 5B (lower row), the patterns could be made to appear significantly more similar, thus revealing the consistency in the underlying attentional topography. (Note that segments with nonsignificant effects may be colored in these adjusted maps.) In contrast, we found that even large adjustments of the color scale could not make the patterns from different subjects look similar to each other.

To quantify these consistencies, we performed a spatial cross-correlation analysis to compare the similarities of patterns obtained within subjects versus between subjects. First, ROImaps from four to eight scan runs per subject were individually normalized with respect to the mean response for the attended target segment. We then computed all possible pairwise cross correlations of the ROImaps for each individual subject (average $r = .60$, $SE = 0.065$). Next, we computed the set of all possible pairwise correlations of ROImaps across different subjects (average $r = .34$, $SE = 0.016$). Finally, the data values from all segments, all repetitions, and all subjects were repeatedly scrambled and randomly assigned to the 18 stimulus segments using Monte Carlo simulation techniques. One thousand pairs of these randomly scrambled patterns were then spatially cross-correlated to estimate the likelihood of obtaining correlations of a given magnitude by chance (average $r = .01$, $SE = 0.0084$).

The results of this analysis are summarized in Figure 5C. The mean values for the five within-subject cross correlations were significantly different from zero. The average within-subject correlation was significantly higher than the between-subject correlations (.60 vs. .32 values), with an overall difference of .26 (t test = 10.5, $p < .001$, two-tailed), and this was true on an individual basis for four of the five subjects. Both within- and between-subject correlations were significantly different from the randomized patterns, the latter being effectively zero ("Random" in Figure 5C). These results support the idea that (1) there is some similarity between individuals that undoubtedly reflects the consistent "hot spot" at the attended target, but that (2) there is an additional level of consistency within each individual that likely reflects idiosyncratic variations on the common theme.

We were concerned that the variations in the individual patterns might reflect poor attentional control. For example, irregularities in these patterns may have been due to attention wandering in this relatively easy task, in which responses were only required every 2 sec. To control for poor attentional stability, we used an alternate, more demanding attentional task on the basis of the widely accepted Rapid Serial Visual Presentation (RSVP) paradigm (Krueger & Shapiro, 1979; Mitchell, 1979). In such tasks, the subject detects relatively infrequent targets embedded in a series of rapidly presented distracter conditions. This is thought to create very high attentional demand, thereby minimizing the possibility for attentional shifts away from the task. In our paradigm, the dartboard-like stimulus remained the same, but subjects performed an RSVP task in which "orange vertical" was the infrequently occurring target conjunction to be detected within a rapid stream of other conjunctions at the cued location. Trials were

presented at a rate of 2.5 per second, which was the fastest rate at which subjects could perform reliably. To ensure adequate response time, the target conjunction always appeared at least eight trials after the previous occurrence, for an average of 12.5 occurrences per 100 trials. Performance was considerably above chance for an average of 74% correct detection and an average false positive rate of less than one per hundred trials. Thus, the task was challenging, but not impossible, and required a high level of vigilance.

ROImaps for five subjects, who performed both the original task and the RSVP task in separate sessions, are illustrated in Figure 6A and B, respectively. Although the ROImaps did vary across the two tasks, there was no evidence that the RSVP task consistently produced more focused maps. Attentional effects still spread to adjacent segments and to some distant segments (e.g., Subject 4, Figure 6B). This was true even for scan runs from the same subject in which performance was very good (>90% correct) or moderate (approx. 75% correct).

Next, another concern was that the idiosyncratic aspects of the topography revealed by BOLD fMRI might reflect an anomalous vascular pattern or some other anatomical or physiological irregularity within the cortical tissue itself. If true, such fixed irregularities should also appear in ROImaps of activation evoked by the target segment itself presented in isolation, while attention is directed to the fixation point. To test this, we presented the target segment alone in a blocked design while participants were required to perform a fixation point "dimming" task continuously throughout the scan. As illustrated in Figure 6C, the resulting average ROImap, as well as the ROImaps of individual subjects, typically showed a tighter focus than the ROImaps of the attention conditions (compare yellow zones in Figure 6B vs. Figure 6C). Moreover, activation in the field opposite the flashed target segment was either lacking or was at a very low level in all subjects. In only one case (Subject 2) did strong activation produced by the target segment spread to an adjacent segment (lower-left neighbor). Finally, two subjects (2 and 4) exhibited suppression in the field opposite the target, an effect that was of opposite sign to that observed in attentional patterns. Together, these results suggested that it was unlikely that the complex attentional topographies we observed had fixed anatomical or physiological origins.

We were also interested in which visual areas might be contributing to the idiosyncratic patterns. For example, it was possible that there would be a tight ipsilateral focus in medial regions such as V1/V2 and a more diffuse pattern including contralateral representation in higher visual regions in the ventral occipital cortex. Therefore, we made separate ROImaps for the medial occipital cortex, including primarily V1/V2, and for ventral occipital regions that likely included V3v (aka VP) and V4v, and probably portions of other ventral areas as well (there was not a sufficient number of voxels within each individual visual area to create ROImaps separately for each of them). The corresponding group-average ROImaps are shown in Figure 6D ("medial" vs. "ventral," respectively) for both the attend-left and attend-right target conditions. The maps computed from the medial and ventral subregions tend to have overall weaker effects due to the smaller sample of voxels contributing to the separate maps. On the whole, the ROImaps from ventral visual areas tend to have stronger effects compared to those from medial areas, as reported previously (Brefczynski & DeYoe, 1999a). Spread of attentional effects to nonattended segments and significant contralateral foci are seen in both medial and ventral ROImaps, although the degree of detailed correspondence is difficult to assess due to the low amplitude of the effects.

Experiment 2: Attentional Distribution at Different Eccentricities

Figure 7A and B shows a set of average AFMaps and ROImaps for five subjects who attended to targets at each of four different eccentricities. The locations and sizes of the targets were scaled in proportion to eccentricity and were cued successively in a temporal phase mapping fMRI paradigm (see Methods: Stimulus and Task for Experiment 2 for details). Note that the

color scales of these maps do not include negative (blue) values. It is an inherent property of the temporal phase mapping design that positive (enhancing) responses associated with each target location will also appear as negative (anticorrelated) responses at target locations cued one-half cycle later. To avoid such confusion, only positive responses are displayed in the maps shown here.

As in Experiment 1, the average fMRI amplitude was strongest at or near each attended target location but spread significantly to nearby targets, and sometimes to more distant targets. The spread of activation appeared to increase dramatically with eccentricity. However, close examination of the degree of dispersion at the same eccentricity as the target suggested a more uniform effect. To examine this issue quantitatively, we used the AFMaps to calculate the dispersion of the most strongly activated voxels (top 250) relative to the center of each attended target location. Dispersion was computed as the mean distance of AFMap symbols from the target center expressed in degrees of visual angle within the field. Because we were mainly interested in the spread of the "hot spot" associated with the attended target, symbols in the hemifield opposite the target that were not part of the "hot spot" were not included to avoid having a small number of highly displaced data points skew the results. As shown in Figure 7C, the mean dispersion can be seen best in the ROImaps (Figure 7B), the spread of attention increased approximately linearly from 3.5° to 14.1° with a slope of 0.54° of dispersion per degree of eccentricity.

The apparent increase in dispersion of attentional effects with eccentricity does not take into account the increase in target size with eccentricity as illustrated schematically in Figure 7D. To adjust for this, we replotted the ROImaps onto a rectangular, rather than polar, grid that equated the areas of the stimulus segments (Figure 7E, green squares correspond to target segment boundaries). In this format, the spread of enhancement around the attended target appeared much more similar across eccentricities than the apparent spread depicted in Figure 7B. This is also seen quantitatively in Figure 7F for which the dispersion values from Figure 7C were normalized with respect to target segment width. The resulting ratios are quite uniform except for the slightly elevated value for most central eccentricity. This result was also confirmed using an alternate technique to compute the dispersion from the ROImap data (results and details of the analysis are provided in on-line Supplemental Figure 2).

DISCUSSION

Summary

In Experiment 1, sustained attention to a single eccentric target evoked a pattern of fMRI activation that was concentrated in the retinotopically corresponding portions of the occipital visual cortex. In cortical flat maps, this activation appeared as a swath of activation running through all retinotopic visual areas, with the highest intensities typically in the ventral cortex. The parietal cortex tended to show bilateral activation, with stronger activation contralateral to the attended target, consistent with recent studies (Huddleston & DeYoe, 2007; Silver, Ress, & Heeger 2005). We designed AFMap and ROImap methods to provide a detailed picture of how the cortical pattern of attentional enhancement relates to the observer's field of view and to features of the stimulus display. AFMaps showed that attention directed to a single right or left target modulated voxels that retinotopically represented the task-relevant locations, but also affected some voxels representing nearby and sometimes distant locations. Attentional effects at multiple locations have been seen in other studies in which subjects were simultaneously cued multiple targets (VanRullen et al., 2007; McMains & Somers, 2005). However, our results show that the attentional spotlight can have a complex topography even when attention is focused on just one target. Perhaps our most surprising result from this experiment was the documentation of consistent individual variations in attentional topography. Further analysis confirmed that these patterns were present in both medial and

ventral retinotopic occipital cortex, and were not a result of task difficulty or vascular effects. In addition, this attentional topography differed from the pattern of stimulus-driven activity generated by the target segment itself and typically was more diffuse.

Experiment 2 showed that spatially specific attentional modulation could occur at all eccentricities, for targets located within 21° of the fovea. Within the visual field, the spatial dispersion of attentional activation increased approximately linearly with eccentricity. However, the size of targets in this experiment was also intentionally scaled with distance from the center of gaze to compensate for expected changes in "cortical magnification" known to scale with eccentricity (Wolfe, O'Neill, & Bennett, 1998; Sereno et al., 1995; Cowey & Rolls, 1974). As a result, normalizing the dispersion values with respect to target width provided a measure of the attentional dispersion roughly as it would appear in cortical space. The result was a nearly constant attentional dispersion across eccentricities, thereby suggesting that, *within the cortex*, the attentional window was roughly constant in size, at least for these stimulus/task conditions. (The small increase in dispersion at the most foveal location may reflect scaling failures near the center of gaze.) From a neurophysiological point of view, our results do not provide evidence for a major loss of cortical spatial specificity at peripheral eccentricities although, phenomenologically as expressed within the observer's field of view, the "spotlight of attention" does become more diffuse in the periphery as has been reported previously (Seiple et al., 2002). Understanding the interaction of cortical attentional effects with the cortical representation of visual space thus reconciles an apparent discrepancy between neurophysiological and psychological accounts of attentional topography.

Methodological Considerations

The picture of attentional topography offered by fMRI necessarily represents a temporal average of the observer's behavior over the duration of the task "blocks." Although this does not provide a millisecond-by-millisecond account of attention, the ability to visualize this "average" topography is, itself, remarkable and informative. Moreover, this average picture is likely to provide a reasonable reflection of many behaviorally relevant features of attention, some previously undiscovered or at least overlooked. When interpreting the results reported here, especially the accounts of complex individual patterns of attentional topography, it is important to note that: (1) The fMRI response is sluggish so that rapid, momentary, lapses of attentional fixation are unlikely to have a major effect on the fMRI signal. (2) Manipulations of the experimental paradigm (e.g., use of an RSVP task) to minimize attentional "wandering" do not systematically alter the results reported here. (3) The unique attentional patterns for individual subjects are significantly repeatable both within session and across months, suggesting that these patterns reflect systematic individual differences. Even if these unique individual patterns do reflect some sort of attentional instability, the pattern of instability is repeatable, perhaps reflecting attentional habits or other factors which, themselves, may be interesting. (4) Behavioral tests of attentional topography using the same stimulus display yield similar results including occasional, isolated foci of enhancement in the field opposite the attended target (DeYoe & Brefczynski, 2001).

Besides the limitations of temporal resolution, the AFMaps illustrated here also may reflect several other potential sources of experimental error. The temporal phase mapping technique used to assign retinotopic coordinates to each brain voxel has its own sources of error and is indicated in the AFMaps by the size of the circle symbols (Saad, 1996). Furthermore, there is evidence that fMRI may be relatively less sensitive to inhibitory neural activity (Logothetis, 2002), which, if true, would imply that the attentional patterns observed here might be incomplete or perhaps appear more diffuse than the actual spread of neural enhancement. On the other hand, fMRI may be particularly sensitive to modulatory neuronal signals, and so, may

be the method of choice for examining attentional modulation (Viswanathan & Freeman, 2007; Logothetis, 2003; Heeger & Ress, 2002).

Models of Attention

Space-based Models—Our data yield important information concerning the validity of previous models of spatial attention. For example, attention does not simply enhance visual processing uniformly throughout the cortical representation of a hemifield or a quadrant (Hughes & Zimba, 1987; Rizzolatti, Riggio, Dascola, & Umilta, 1987). Rather, attention can have more precise spatial specificity consistent with a spotlight or zoom lens model (Klein & McCormick, 1989). However, the simple versions of these latter models do not fully account for our results. Attentional topography was often complex, sometimes with separate weak secondary foci. Such complexity is not in accord with either spotlight or zoom lens models (Cave & Bichot, 1999; Eriksen & Yeh, 1985). When the complex topographies of individual subjects are combined into a single average, the resulting pattern conforms well to a gradient model of attention in which cortical enhancement is strongest at the attended target location and decreases gradually with distance (Eriksen & St James, 1986; Downing & Pinker, 1985; Eriksen & Yeh, 1985; Shaw, 1978; Shaw & Shaw, 1977). In this context, it is important to note that many psychophysical studies have based their conclusions and models on data averaged across multiple subjects, thereby deemphasizing the importance of individual variations. However, close scrutiny of at least one previously published study also reveals individual variation that may have been overlooked (Hughes & Zimba, 1987).

Object-based Models—Various behavioral, single-unit, fMRI, and EEG studies predict that the overall topography of attentional enhancement should be strictly confined to the boundaries of an attended object (Martinez, Teder-Salejarvi, & Hillyard, 2007; He, Fan, Zhou, & Chen, 2004; Muller & Kleinschmidt, 2003; Luck, Chelazzi, Hillyard, & Desimone, 1997; Desimone & Duncan, 1995; Egly, Driver, & Rafal, 1994; Heinze et al., 1994; Desimone & Schein, 1987; Duncan, 1984). In our experiments, each segment in the dartboard array might be considered to be an individual object, separated from others by gray borders (Figure 1C). Although we did observe that attentional enhancement typically was strongest within the boundaries of the attended segment, it was not strictly confined there. In this respect, it is important to note that the fMRI activation that was driven by the attended target, presented in isolation, also spread beyond the strict retinotopic confines of the stimulus, although it is unclear if this reflects inaccuracies in determining the retinotopic representation of each voxel, diffuseness in the hemodynamic mechanisms underlying the BOLD signal or true diffuseness in the neural representation of an object with sharp boundaries. In any event, the dispersion of attentional effects was typically more diffuse than the dispersion of the stimulus driven activity consistent with the inference that they extended beyond the boundaries of the attended object, however, those boundaries might be represented in the cortex. Interestingly, studies using object-based stimuli have typically shown more spatially specific effects (Seiple et al., 2002; Slotnick, Hopfinger, Klein, & Sutter, 2002) compared to studies not using object-based stimuli (i.e., flash detection in an otherwise empty field; Hughes & Zimba, 1987; Rizzolatti et al., 1987). These results suggest that both spatial location and object effects may alternately, or conjointly, influence the attentional distribution (Martinez et al., 2007; Arrington, Carr, Mayer, & Rao, 2000; Motter & Belky, 1998; Lavie & Driver, 1996; Motter, 1993) or that both types of effects may arise from a common mechanism (Logan, 1996). Consequently, the current experiments do not provide a definitive conclusion with regard to this issue.

Attentional Style

Our results suggest that each observer has an attentional topography that reflects a common pattern seen almost universally but also may have their own idiosyncratic “attentional style” manifested as unique variations on this common theme. We refer to the concept of attentional

style as a specific instance of the more general, and widely accepted, notion of "cognitive style" (Broverman, 1960). The unique topographical features of each individual's AFMap do not seem to reflect fixed physiological features or anomalous vascular innervation because such features would be expected to affect stimulus driven activation patterns in a similar manner, but did not. Moreover, although the unique attentional patterns are generally repeatable, they do vary somewhat over time, again contrary to the idea of a fixed physiological basis.

An intriguing alternative is that the spatial aspects of attentional style may reflect behavioral habits or environmental consistencies that are specific to each individual's life experience. For example, there may be a consistent, but unique, layout of features inside an individual's car such that the position of the rearview mirror with respect to the road causes them to form a habitual attentional scanning pattern. Over time, this pattern may become a repeatable, but subtle, characteristic of the individual's more general use of attention. Thus, the complete pattern of each individual's attentional topography may reflect a common neurophysiological "instrument" played upon by each person's unique experience.

Supplementary Material

Refer to Web version on PubMed Central for supplementary material.

Acknowledgments

We thank Jed Mathis and Jon Wieser for assistance in figure production and data collection, and Doug Ward and Dr. Ray Hoffman for help with statistical analysis. Funding from NIH grant EB00843 to E. DeYoe, NIH grant RR00058 to the Medical College of Wisconsin.

References

Arrington CM, Carr TH, Mayer AR, Rao SM. Neural mechanisms of visual attention: Object-based selection of a region in space. Journal of Cognitive Neuroscience 2000;12:106–117. [PubMed: 11506651]

Bandettini PA, Jesmanowicz A, Wong EC, Hyde JS. Processing strategies for functional MRI of the human brain. Magnetic Resonance in Medicine 1993;30:161–173. [PubMed: 8366797]

Brefczynski J, Lewis J, DeYoe EA. Topography of attentional enhancement in human occipital and parietal cortex. Society of Neuroscience Abstracts 1999;25:287.

Brefczynski JA, DeYoe EA. A physiological correlate of the "spotlight" of visual attention. Nature Neuroscience 1999a;2:370–374.

Brefczynski JA, DeYoe EA. Visual field mapping of the "spotlight" of visual attention. Neuroimage 1999b;9:775.

Broverman DM. Cognitive style and intra-individual variation in abilities. Journal of Personality 1960;28:240–255. [PubMed: 13804869]

Cave KR, Bichot NP. Visuospatial attention: Beyond a spotlight model. Psychonomic Bulletin & Review 1999;6:204–223. [PubMed: 12199208]

Cowey A, Rolls ET. Human cortical magnification factor and its relation to visual acuity. Experimental Brain Research 1974;21:447–454.

Cox RW. AFNI: Software for analysis and visualization of functional magnetic resonance neuroimages. Computers and Biomedical Research 1996;29:162–173. [PubMed: 8812068]

Cox, RW. What does the "intensity" computed by FIM mean?. 2005. Available at http://afni.nimh.nih.gov/afni/doc/faq/35/view?searchterm=afni200.ps

Cox RW, Jesmanowicz A, Hyde JS. Real-time functional magnetic resonance imaging. Magnetic Resonance in Medicine 1995;33:230–236. [PubMed: 7707914]

Desimone R, Duncan J. Neural mechanisms of selective visual attention. Annual Review of Neuroscience 1995;18:193–222.

Desimone R, Schein SJ. Visual properties of neurons in area V4 of the macaque: Sensitivity to stimulus form. Journal of Neurophysiology 1987;57:835–868. [PubMed: 3559704]

DeYoe, EA.; Brefczynski, JA. The visual field representation of cortical attentional enhancement; 3rd Annual Vision Research Conference: Pre-attentive and Attentive Mechanisms in Vision; Ft. Lauderdale. 1999. p. 132

DeYoe EA, Brefczynski JA. Visual field topography of spatial attention: Psychophysics. Society of Neuroscience Abstracts 2001;27:574.2.

DeYoe EA, Brefczynski-Lewis JA, Datta R, Huddleston W. The expression and control of attentional topography in human visual cortex. Human Brain Mapping Abstracts 2004;22:TH28.

DeYoe EA, Carman G, Bandettini P, Glickman S, Wieser J, Cox R, et al. Mapping striate and extrastriate visual areas in human cerebral cortex. Proceedings of the National Academy of Sciences, U.S.A 1996;93:2382–2386.

Downing, CJ.; Pinker, S., editors. The spatial structure of visual attention. Hillsdale, NJ: Erlbaum; 1985.

Duncan J. Selective attention and the organization of visual information. Journal of Experimental Psychology: General 1984;113:501–517. [PubMed: 6240521]

Egly R, Driver J, Rafal RD. Shifting visual attention between objects and locations: Evidence from normal and parietal lesion subjects. Journal of Experimental Psychology: General 1994;123:161–177. [PubMed: 8014611]

Eriksen CW, St James JD. Visual attention within and around the field of focal attention: A zoom lens model. Perception & Psychophysics 1986;40:225–240. [PubMed: 3786090]

Eriksen CW, Yeh YY. Allocation of attention in the visual field. Journal of Experimental Psychology: Human Perception and Performance 1985;11:583–597. [PubMed: 2932532]

Gandhi SP, Heeger DJ, Boynton GM. Spatial attention affects brain activity in human primary visual cortex. Proceedings of the National Academy of Sciences, U.S.A 1999;96:3314–3319.

Gobell JL, Tseng CH, Sperling G. The spatial distribution of visual attention. Vision Research 2004;44:1273–1296. [PubMed: 15066391]

He X, Fan S, Zhou K, Chen L. Cue validity and object-based attention. Journal of Cognitive Neuroscience 2004;16:1085–1097. [PubMed: 15298794]

Heeger DJ, Ress D. What does fMRI tell us about neuronal activity? Nature Reviews Neuroscience 2002;3:142–151.

Heinze HJ, Luck SJ, Munte TF, Gos A, Mangun GR, Hillyard SA. Attention to adjacent and separate positions in space: An electrophysiological analysis. Perception & Psychophysics 1994;56:42–52. [PubMed: 8084731]

Huddleston WE, Deyoe EA. The representation of spatial attention in human parietal cortex dynamically modulates with performance. Cerebral Cortex 2008;18:1272–1280. [PubMed: 17962221]

Hughes HC, Zimba LD. Spatial maps of directed visual attention. Journal of Experimental Psychology: Human Perception and Performance 1985;11:409–430. [PubMed: 3161984]

Hughes HC, Zimba LD. Natural boundaries for the spatial spread of directed visual attention. Neuropsychologia 1987;25:5–18. [PubMed: 3574650]

Jesmanowicz A, Bandettini PA, Hyde JS. Single-shot half k-space high resolution gradient-recalled EPI for fMRI at 3 Tesla. Magnetic Resonance in Medicine 1998;45:595–604.

Jesmanowicz A, Wong EC, DeYoe EA, Hyde JS. Method to correct anatomic distortion in echo planar images. Proceedings of the Society of Magnetic Resonance in Medicine 1992;2:4260.

Klein R, McCormick P. Covert visual orienting: Hemifield-activation can be mimicked by zoom lens and midlocation placement strategies. Acta Psychologica 1989;70:235–250. [PubMed: 2750553]

Krueger LE, Shapiro RG. Letter detection with rapid serial visual presentation: Evidence against word superiority at feature extraction. Journal of Experimental Psychology: Human Perception and Performance 1979;5:657–673. [PubMed: 528966]

LaBerge D. Spatial extent of attention to letters and words. Journal of Experimental Psychology: Human Perception and Performance 1983;9:371–379. [PubMed: 6223977]

Lavie N, Driver J. On the spatial extent of attention in object-based visual selection. Perception & Psychophysics 1996;58:1238–1251. [PubMed: 8961834]

Logan GD. The CODE theory of visual attention: An integration of space-based and object-based attention. Psychological Review 1996;103:603–649. [PubMed: 8888649]

Logothetis NK. The neural basis of the blood-oxygen-level-dependent functional magnetic resonance imaging signal. Philosophical Transactions of the Royal Society of London, Series B, Biological Sciences 2002;357:1003–1037.

Logothetis NK. The underpinnings of the BOLD functional magnetic resonance imaging signal. Journal of Neuroscience 2003;23:3963–3971. [PubMed: 12764080]

Luck SJ, Chelazzi L, Hillyard SA, Desimone R. Neural mechanisms of spatial selective attention in areas V1, V2, and V4 of macaque visual cortex. Journal of Neurophysiology 1997;77:24–42. [PubMed: 9120566]

Martinez A, Teder-Salejarvi W, Hillyard SA. Spatial attention facilitates selection of illusory objects: Evidence from event-related brain potentials. Brain Research 2007;1139:143–152. [PubMed: 17288996]

McMains SA, Somers DC. Processing efficiency of divided spatial attention mechanisms in human visual cortex. Journal of Neuroscience 2005;25:9444–9448. [PubMed: 16221854]

Mitchell DC. The locus of the experimental effects in the rapid serial visual presentation (RSVP) task. Perception & Psychophysics 1979;25:143–149. [PubMed: 432099]

Motter BC. Focal attention produces spatially selective processing in visual cortical areas V1, V2, and V4 in the presence of competing stimuli. Journal of Neurophysiology 1993;70:909–919. [PubMed: 8229178]

Motter BC, Belky EJ. The zone of focal attention during active visual search. Vision Research 1998;38:1007–1022. [PubMed: 9666983]

Muller NG, Kleinschmidt A. Dynamic interaction of object- and space-based attention in retinotopic visual areas. Journal of Neuroscience 2003;23:9812–9816. [PubMed: 14586009]

Posner MI, Snyder CRR, Davidson BJ. Attention and the detection of signals. Journal of Experimental Psychology 1980;109:160–174. [PubMed: 7381367]

Rizzolatti G, Riggio L, Dascola I, Umilta C. Reorienting attention across the horizontal and vertical meridians: Evidence in favor of a premotor theory of attention. Neuropsychologia 1987;25:31–40. [PubMed: 3574648]

Saad, Z. Doctoral dissertation. Milwaukee: Department of Bioengineering, Marquette University; 1996. Temporal properties of fMRI signals.

Saad, Z. Temporal variability in fMRI response to visual stimulation in human brain. Milwaukee, WI: Bioengineering Department, Marquette University; 2000. p. 213

Saenz M, Buracas GT, Boynton GM. Global feature-based attention for motion and color. Vision Research 2003;43:629–637. [PubMed: 12604099]

Seiple W, Clemens C, Greenstein VC, Holopigian K, Zhang X. The spatial distribution of selective attention assessed using the multifocal visual evoked potential. Vision Research 2002;42:1513–1521. [PubMed: 12074946]

Sereno MI, Dale AM, Reppas JB, Kwong KK, Belliveau JW, Brady TJ, et al. Borders of multiple visual areas in humans revealed by functional MRI. Science 1995;268:889–893. [PubMed: 7754376]

Shaw ML. A capacity allocation model for reaction time. Journal of Experimental Psychology: Human Perception and Performance 1978;4:586–598.

Shaw ML, Shaw P. Optimal allocation of cognitive resources to spatial locations. Journal of Experimental Psychology: Human Perception and Performance 1977;3:201–211. [PubMed: 864393]

Silver MA, Ress D, Heeger DJ. Topographic maps of visual spatial attention in human parietal cortex. Journal of Neurophysiology 2005;94:1358–1371. [PubMed: 15817643]

Slotnick SD, Hopfinger JB, Klein SA, Sutter EE. Darkness beyond the light: Attentional inhibition surrounding the classic spotlight. NeuroReport 2002;13:773–778. [PubMed: 11997685]

Tootell RBH, Hadjikhani N, Hall EK, Marrett S, Vanduffel W, Vaughan JT, et al. The retinotopy of spatial attention. Neuron 1998;21:1409–1422. [PubMed: 9883733]

Treisman AM. Perceptual grouping and attention in visual search for features and for objects. Journal of Experimental Psychology: Human Perception and Performance 1982;8:194–214. [PubMed: 6461717]

Van Essen DC, Lewis JW, Drury HA, Hadjikhani N, Tootell RBH, Bakircioglu M, et al. Mapping visual cortex in monkeys and humans using surface-based atlases. Vision Research 2001;41:1359–1378. [PubMed: 11322980]

VanRullen R, Carlson T, Cavanagh P. The blinking spotlight of attention. Proceedings of the National Academy of Sciences, U.S.A 2007;104:19204–19209.

Viswanathan A, Freeman RD. Neurometabolic coupling in cerebral cortex reflects synaptic more than spiking activity. Nature Neuroscience 2007;10:1308–1312.

Wolfe JM, O'Neill P, Bennett SC. Why are there eccentricity effects in visual search? Visual and attentional hypotheses. Perception & Psychophysics 1998;60:140–156. [PubMed: 9503918]

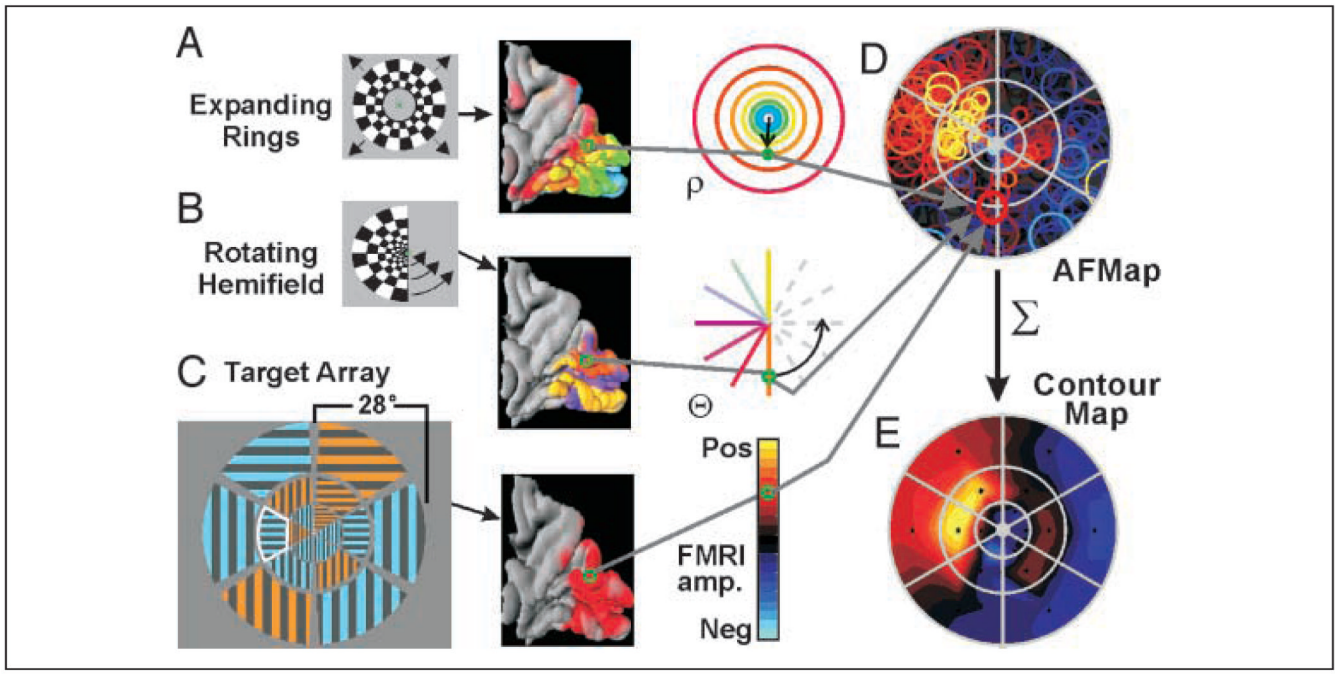

Figure 1.

Construction of AFMaps and ROImaps. A flickering checkered annulus (A) and a rotating hemifield (B) were used to determine the stimulus eccentricity (rho) and angular position (theta) that maximally activated each responsive voxel in the brain and to create color-coded maps displayed on a 3-D model (medial view, posterior to right) of the cortical surface within the occipital lobe and adjacent portions of the parietal cortex. Color codes for eccentricity and polar angle as indicated in the third column (for angular position, orange = lower vertical meridian [VM]; yellow = upper VM; purple = horizontal meridian). The preferred *rho* and *theta* position for each voxel were used to place circle symbols at corresponding positions on a chart of the visual field (gray arrows, D). Size of symbols provides a measure of experimental error in estimating retinotopic coordinates for each voxel. Color of symbols encodes amplitude of attention-related fMRI activation recorded during separate task in which subjects attended to a verbally cued target segment within a dartboard-like array of striped and colored segments. Here, the cued segment is indicated by a white outline that was not part of the actual stimulus. The pattern of circles for all active voxels shows distribution of attention-related activity, or attentional field map (AFMap), as it would appear within the observer's field of view and relative to the target array (gray grid in D). (E) To compare attentional effects for different target segments, the fMRI amplitudes of all voxels representing each segment (circles whose centers were within a segment's boundaries) were averaged and the resulting values were used to color code the center points of each segment (small black asterisks) on a second map with colors interpolated between data points by fitting with a smooth surface viewed here as a contour map (a.k.a. region-of-interest map ROImap).

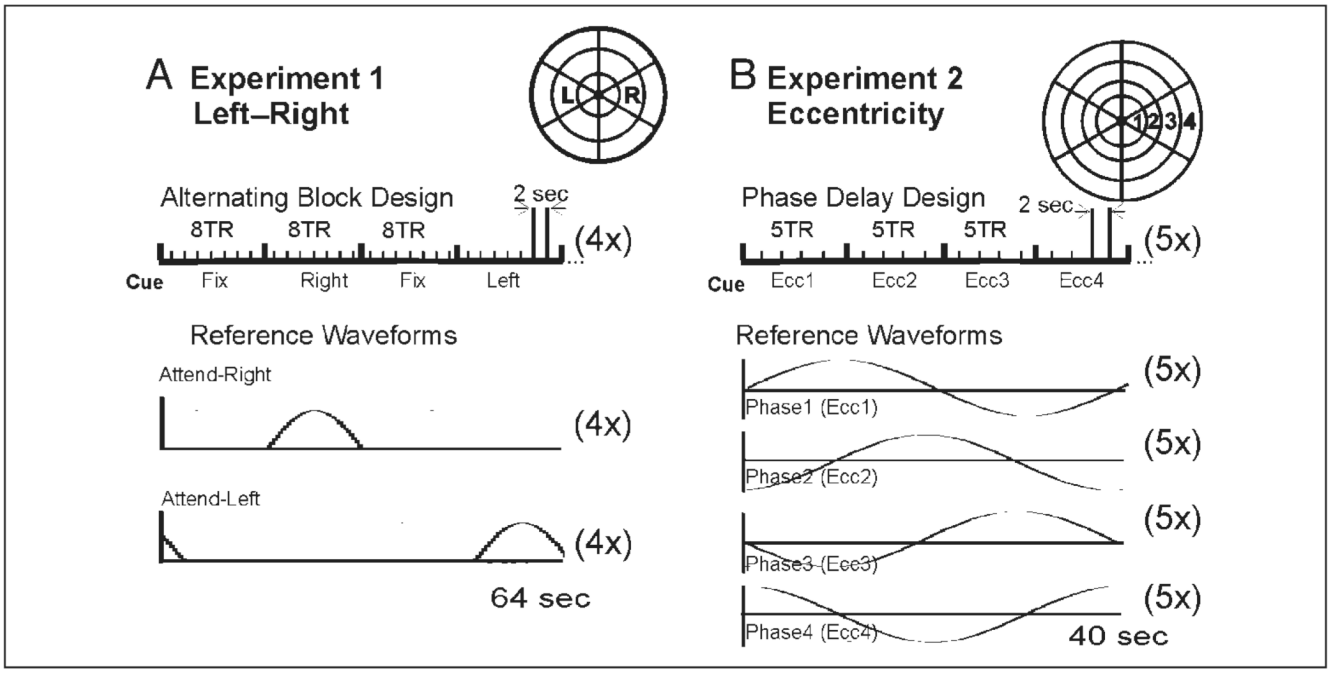

Figure 2.

Task timing. (A) Experiment 1—left–right target experiment: 16-sec blocks of passive fixation (Fix) alternated with blocks of directed attention to the right (Right) or left (Left) targets (schematic of target array in upper right of A). Each full cycle of "Fix, Right, Fix, Left" was repeated four times per scan run. MRI imaging TR = 2 sec. Lower graphs: Reference waveforms used to detect activation for attend-right or attend-left blocks. (B) Experiment 2—Eccentricity sequence: Every 10 sec, subjects shifted attention successively to each of four targets increasing in eccentricity (schematic in upper right of B) repeated five times per scan run. In this temporal phase mapping paradigm, there was no passive fixation period. Subjects just shifted attention from location to location as cued. Lower graphs: Reference waveforms used to detect activation for each eccentricity (each phase delay).

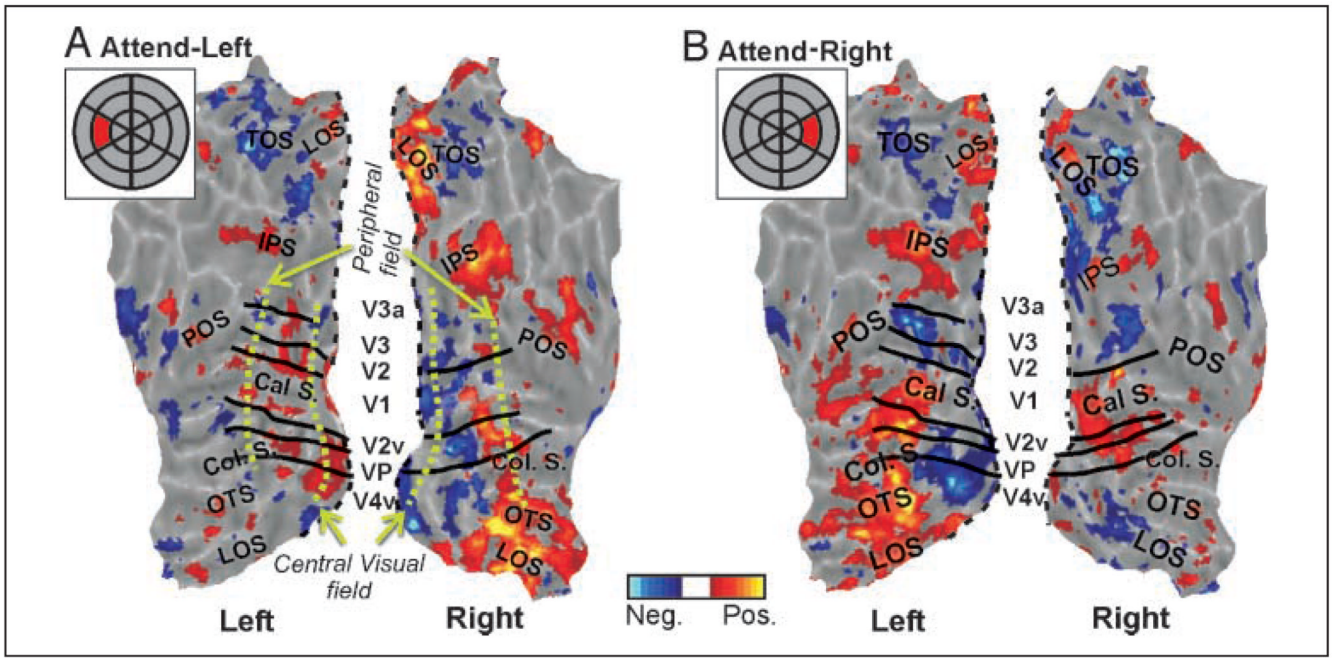

Figure 3.

Attention-related fMRI activation represented on flatmaps of the occipital–parietal cortex for the attend-left (A) and the attend-right (B) conditions for a single subject. Insets show schematic stimulus array with cued target in red. fMRI color scale is similar to Figure 2. Some visual area boundaries are shown in black and labeled in the space between the two hemispheres. Black dashed line on each map indicates margin of "cut" used to allow unfolding of occipital lobe. Flatmaps use shades of gray to represent gyri (light gray) and sulci (darker grays). Major sulci: calcarine (Cal S.), collateral (Col. S.), occipital temporal (OTS), lateral occipital (LOS), intraparietal sulcus (IPS), transverse occipital (TOS), and parietal occipital (POS). Green dashed lines approximately indicate foveal versus peripheral field representations.

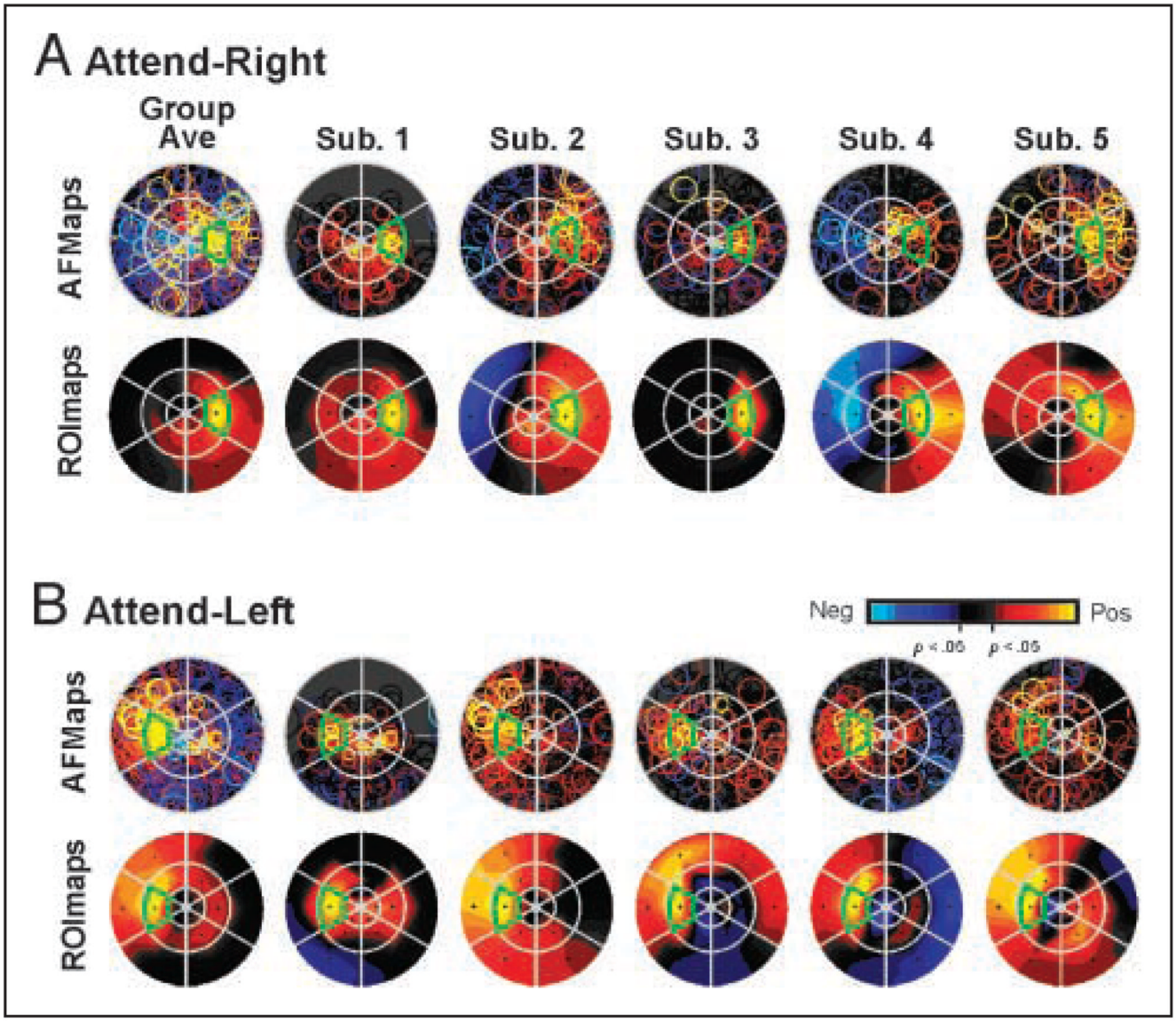

Figure 4.

AFMaps and ROImaps for the attend-right (A) and attend-left (B) conditions of Experiment 1. (See Figure 1 and text for details of flat map construction and interpretation.) "Group Ave" maps represent data pooled from five subjects whose individual maps are show to the right. Note color code for amplitude of fMRI modulation with statistically significant values ($p < .05$) indicated in yellow/red (positive, activating responses) or blue (negative, suppressive responses). Responses that were not significantly different from passive fixation baseline indicated in shades of gray/black.

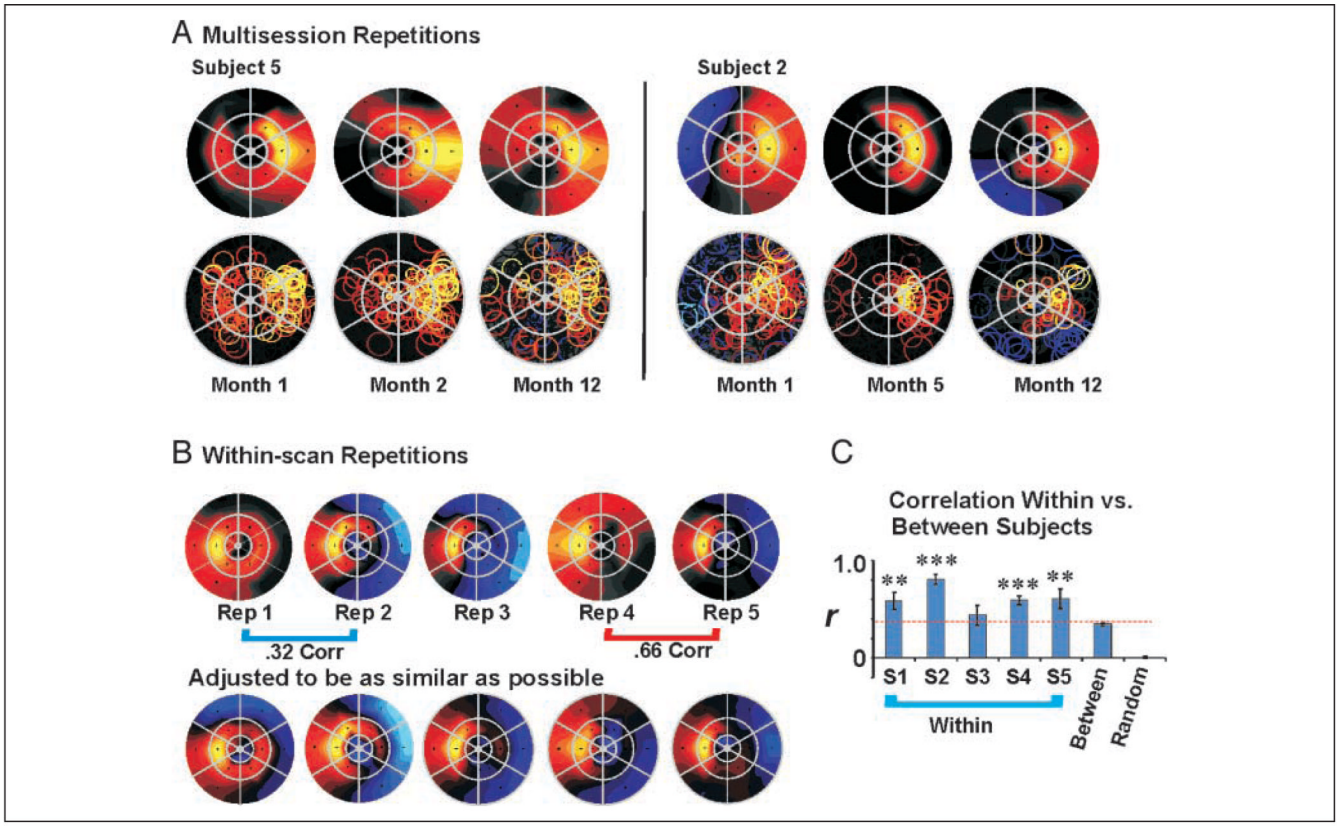

Figure 5.

Consistency of attentional topography. (A) AFMaps for two subjects showing the attend-right condition measured thrice over a 1-year period. Attended target location was middle right segment. Color scale as in Figure 4. (B) Five repeated scans for attend-left condition collected within a single session for one subject (#4 of Figure 4). Maps in B, bottom row maps have colors manually scaled to make topographic similarities more apparent, although gray/black colors may no longer indicate nonsignificant responses (see text). (C) Spatial cross correlation of attentional maps for same (within) or different (between) subjects. S1–S5 = within-subject correlations. Between = between subject correlations. Random = correlations for scrambled data (see text). Correlations within each subject were significantly higher than correlations between subjects (indicated by dotted red line). Correlations of the randomized data were not significantly different from zero. Asterisks indicate significance of individual-subject correlations compared with between-subject correlation in a two-tailed *t* test of Fisher transformed values, **<.01, ***<.005. Although the attentional conditions were the same in all cases, the data were obtained in the context of different experiments.

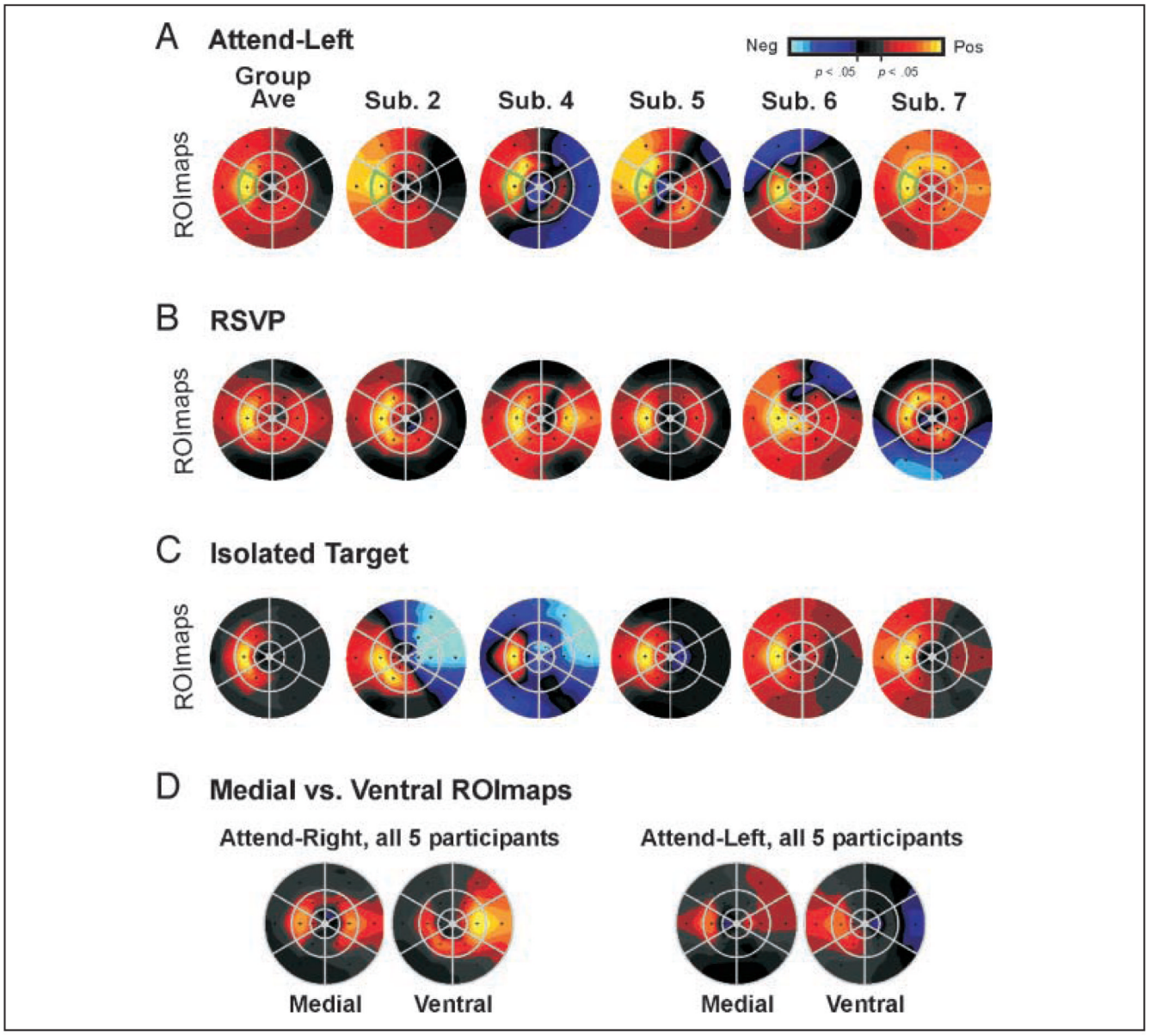

Figure 6.

AFMaps and ROImaps for multiple control conditions for five subjects. (A) Attend-left condition of Experiment 1 as a reference. (B) RSVP task: Subjects detected a rarely occurring color/orientation at the attended target alternated with blocks of passive fixation. Trials presented every 0.4 sec. (C) Isolated target: Target segment presented in isolation against a gray background while subject performed fixation point dimming task continuously through entire scan run. This shows distribution of stimulus-driven activation in contrast to attention-driven activation. (D) ROImaps from the medial versus ventral occipital cortex. Medial = retinotopic areas in and near the calcarine sulcus. Ventral = retinotopic areas in or near the collateral sulcus for the attend-right and attend-left conditions of Experiment 1. Here color scale is normalized to maximum response for the standard ROImap in which all voxels were included, to show relative strengths of activation between regions.

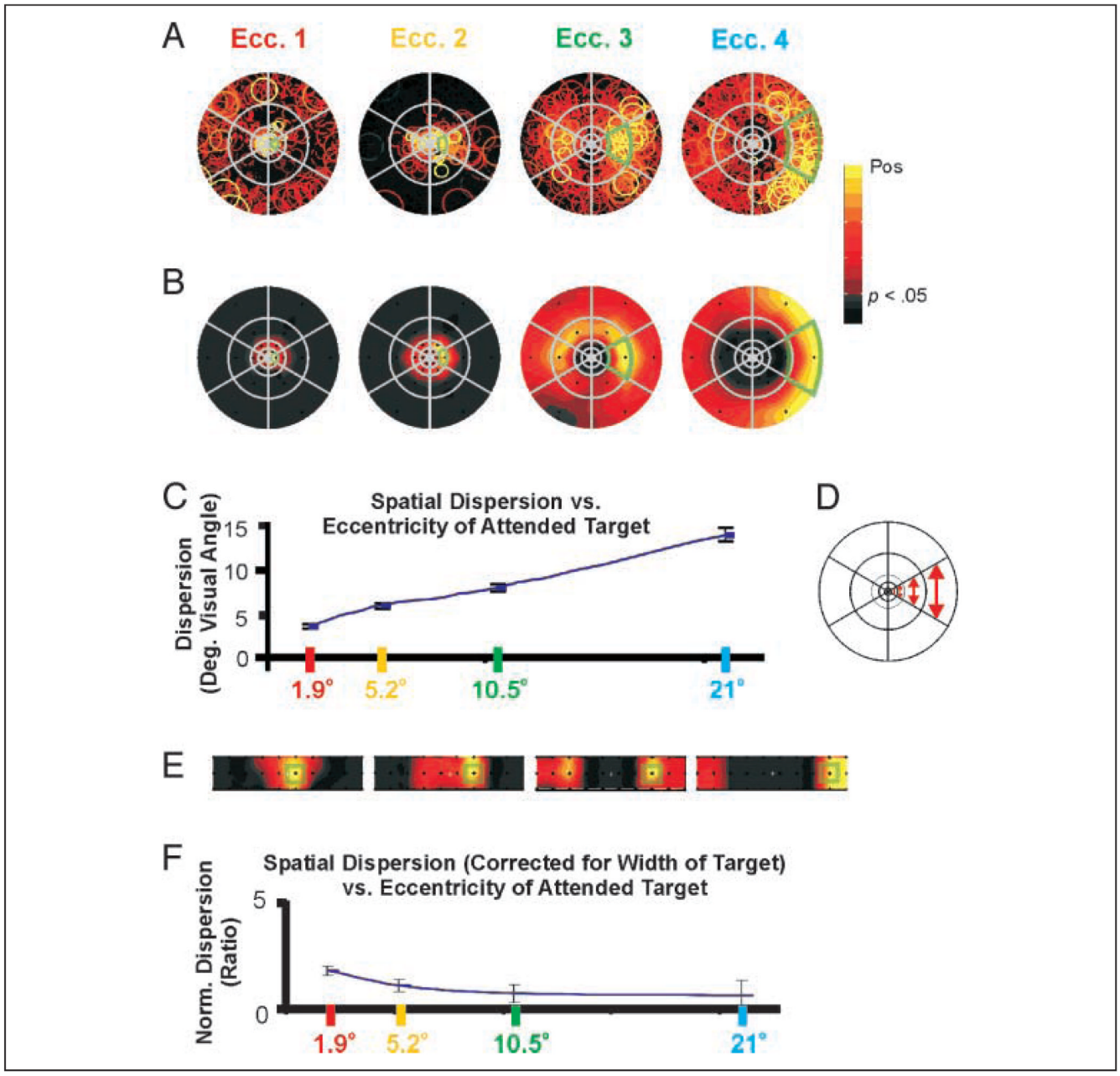

Figure 7.

"Window of attention" increases with eccentricity in visual field but is constant in the cortex: Average (5 subjects) (A) AFMaps and (B) ROImaps for attended targets at four different eccentricities in the visual field. Note that due to large numbers of voxels per region, segments showing active voxels in the AFMaps do not necessarily have a high mean value for the ROImap. (C) Mean dispersion (in degrees of visual angle) versus mean target eccentricity for top 250 voxels having the strongest attention-related signals. (D) Schematic of stimulus array illustrating increase in target size with eccentricity. (E) ROImaps of B spatially transformed to equate for sizes of targets. In all maps, green outlines indicate the relative size and position of the cued target. This transformation roughly compensates for cortical magnification (see text) and provides an approximation of the relative dispersion of attentional effects within the

cortex (V1). (F) Mean dispersion normalized as in E versus target eccentricity. Normalized dispersion is nearly constant with eccentricity, suggesting that size of the attentional "window" in cortical space may be constant. Note: The color scale in these maps excludes negative values because the temporal phase mapping delay design does not permit independent visualization of suppressive effects.